2017-01-0829

Exploration of Turbulent Atomization Mechanisms for Diesel Spray Simulations

Gina M. Magnotti and Caroline L. Genzale

Georgia Institute of Technology

Abstract

The atomization and initial spray formation processes in direct injection engines are not well understood due to the experimental and computational challenges associated with resolving these processes. Although different physical mechanisms, such as aerodynamic-induced instabilities and nozzle-generated turbulence and cavitation, have been proposed in the literature to describe these processes, direct validation of the theoretical basis of these models under engine-relevant conditions has not been possible to date. Recent developments in droplet sizing measurement techniques offer a new opportunity to evaluate droplet size distributions formed in the central and peripheral regions of the spray. There is therefore a need to understand how these measurements might be utilized to validate unobservable physics in the near nozzle-region.

To address this need, we conduct a computational study using 3D CFD simulations in CONVERGE to explore the relationship between the selected primary atomization model and droplet sizes formed in the central and peripheral regions of the spray. Two existing primary atomization models from the literature are studied to characterize the influence of competing aerodynamics and turbulence mechanisms on the spray formation process. We develop and implement a new hybrid primary atomization model to evaluate the influence of the assumed turbulent scaling on the predicted spray structure. Local sensitivity analysis is performed over a wide range of ambient densities, injection pressures and nozzle diameters to compare the response of predicted droplet sizes in different regions of the spray to changes in injection and ambient conditions. Comparison of the predicted spray structure among the three spray models and against available measurements helps identify a set of experimental conditions and measurements that are needed to inform the development of improved atomization and spray breakup models.

Introduction

Even after 60 years of experimental and computational sprays research, the process by which a direct-injected high-pressure liquid fuel jet breaks up into droplets remains unknown. This gap in knowledge stems from the challenge faced by experimentalists [1-6] and computationalists [7-9] alike in simultaneously resolving the large span of length and time scales characterizing the atomization and droplet formation process. As a result, our collective knowledge of the physics governing these processes has been through the experimental observation of macroscopic spray characteristics, such as spray penetration and spreading angle, and microscopic spray details downstream of the atomizing jet, such as droplet size and velocity, and through the indirect validation of spray model predictions against these measurements.

The fuel injection and spray breakup process for engine computational fluid dynamics (CFD) simulations is a challenging computational problem due to the multi-phase, multi-physics, and multi-scale nature of the flow. Several modeling approaches have been used to represent the liquid and gas phases and the exchange of mass, momentum and energy, but the most commonly employed method is the Lagrangian-Eulerian framework [10-12]. In this method, the continuous gas phase is resolved on the Eulerian grid while the liquid phase is modeled by tracking discrete parcels and their evolution using a Lagrangian formulation. Using the "blob" injection method developed by Reitz and Diwakar [13], the injection event is represented by a train of discrete injected parcels which start with a droplet size on the order of the nozzle diameter. Each parcel statistically represents a number of droplets, *N*, that share identical droplet properties (size, temperature, etc.) [14]. Because the liquid phase is not directly resolved on the grid, there is a need to employ sub-models to represent the unresolved physics, such as primary atomization and secondary droplet break up. However, the appropriateness of the physical mechanisms implemented in today's CFD codes to represent these physics remains unknown.

Experimentalists have evaluated a wide array of spray characteristics in the hope of relating spray observables to unobservable near-nozzle spray formation processes. For example, Reitz evaluated the response of the spray spreading angle to changes in fuel viscosity, nozzle geometries, injection and ambient conditions [15]. The data was then compared to the predicted droplet trajectory angle using theoretical scaling of the growth rate of the fastest growing surface wave from linear stability analysis [16]. Even though Reitz acknowledged the influence of additional physical mechanisms on the spray breakup process, such as nozzle-generated cavitation and turbulence [15], good agreement between the theoretical predictions and measured spray angles led to the development of spray atomization models primarily based on the growth of aerodynamic instabilities, as implemented in the widely adopted Kelvin Helmholtz (KH) primary atomization model [17]. However, good agreement was only possible through calibration of the model for every nozzle considered, indicating a lack of physics relating the internal nozzle geometry effects to the spray formation process.

Motivated by the excessive tuning required to match the predicted and measured spreading angle, Huh and Gosman developed a new spray model that linked the spray spreading angle with both internal nozzle flow development and primary atomization [18]. Through an order of magnitude analysis of the possible forces acting on the spray as it exits the nozzle, it was determined that the dominant forces were due to the gas inertia and internal turbulent stresses in the liquid. The importance of the gas inertial force was used to justify the inclusion of the KH instability mechanism in the model. However, it was reasoned that the source of the initial turbulent fluctuations controls the primary atomization length scale, which was assumed to be proportional to the integral turbulence scale, whereas the primary atomization time scale is a weighted average of the turbulence time scale and the KH timescale for the fastest growing wave. Although the model requires the calibration of three model constants, which control the relative contributions of turbulence and aerodynamic instabilities on the atomization time scale and the ultimate breakup rate of the spray, the implemented physics were deemed to be validated through replication of the experimentally observed trends [19-21] for the spreading angle from four different nozzles. Subsequent evaluation of the model was conducted through comparisons of predicted and measured spray tip penetration and far-field droplet size measurements along the spray centerline and periphery at distances of 40 nozzle diameters or larger from the nozzle exit [22]. Although the model was noted to predict the spray observables well, the relative influence of the aerodynamic and turbulence primary atomization models on these spray parameters was not evaluated.

The role of the selected primary atomization model on the predicted spray metrics was extensively studied throughout the body of work conducted by Som and Aggarwal [23-26]. In particular, the primary atomization process was characterized by the resultant distribution of liquid mass and droplet dispersion. Such comparisons were only possible through the use of x-ray radiography measurements, which enabled the quantification of liquid mass distributions, particularly in dense regions of the spray [27-28]. Through the comparison of measured and predicted liquid mass distributions at various locations in the spray, the KH model was found to underpredict droplet dispersion, as indicated by the relatively narrower mass distributions in comparison to the experimental data. The underprediction in droplet dispersion was attributed to the insufficient formation of child droplets from the primary atomization process [24]. As a result, the inclusion of additional primary atomization mechanisms, such as turbulence- and cavitation-induced breakup was motivated by the need to improve model predictions of droplet dispersion. The addition of these physics was further supported through the inability of the KH model to predict the expected trends of injector nozzle geometry on droplet dispersion [24, 26]. The hybrid spray model that was developed form this work, called the KH Aerodynamics-Cavitation-Turbulence (KH-ACT) model, resulted in the improved prediction of spray characteristics across non-vaporizing, vaporizing, and combusting conditions characteristic of conventional diesel operation (ρ_g greater than 7 kg/m^3, ρ_f/ρ_g less than 100) [25-26].

However, for lower ambient density environments approaching atmospheric conditions (ρ_g less than 7 kg/m^3, ρ_f/ρ_g greater than 100) which characterize low temperature combustion concepts, the KH-ACT model was only observed to produce marginal improvements over the KH model for predictions of liquid length and vapor penetration [25]. Although the influence of the employed primary atomization model was shown to have diminished influence on the spray formation process under vaporizing conditions [24-25], this predicted discrepancy might suggest that the scalings employed in the turbulence model did not sufficiently enhance droplet formation and droplet dispersion. Indeed, the turbulent atomization process in the KH-ACT model is assumed to scale with the turbulence integral scaling [24]. It may be possible that the employment of a different turbulence scaling that results in the formation of smaller droplets could improve the predictive capability of the KH-ACT model under vaporizing conditions. However, to the best of the authors' knowledge, no computational study has yet demonstrated the influence of the assumed turbulence scaling of the primary atomization model on the predicted spray formation process. Spray modeling studies that explore the influence of the employed primary atomization model and assumed scalings on the predicted spray structure at these challenging low ambient density conditions, in concert with comparison against available spray measurements, could help address this current modeling deficiency among existing spray models in the literature.

As spray diagnostics continue to advance and characterize processes closer to the primary atomization region of the spray, it is necessary to understand how these measurements can be employed to address remaining questions regarding the appropriate length and time scales describing the atomization and spray formation process. For example, high magnification holographic imaging experiments have helped inform the theory underlying turbulence-driven primary atomization for liquid jets [29-30]. This imaging technique has been applied to sprays to quantify the breakup size scales of many liquid jet configurations, providing quantitative validation of turbulence-based scaling within the inertial subrange for jets under atmospheric conditions, where ρ_f/ρ_g ($\hat{\rho}$) are less than 500. Limited experiments under higher ambient densities (up to $\hat{\rho}$ of around 100) showed some evidence of aerodynamic forces assisting the breakup process, but breakup still scaled with liquid turbulence properties [29], suggesting that the mechanism responsible for inducing initial jet instabilities was still turbulence at moderate ambient densities. Questions remain on how the theory describing aerodynamic assisted turbulent breakup, as proposed by Wu and Faeth, can be extended to $\hat{\rho}$ conditions greater than 100.

In pursuit of a unifying primary atomization theory that can be employed throughout the engine cycle across a wide range of ambient and injection conditions, we implement a new hybrid primary atomization model, called the KH-Faeth model. Similar to the KH-ACT model, the KH-Faeth model allows for the competition between aerodynamic and turbulent primary atomization, but the characteristic turbulent atomization length scale is smaller than the assumed integral length scale in the KH-ACT model [24]. Comparison of model predictions between the KH-ACT and KH-Faeth models across a wide range of injection and ambient conditions will allow for the influence of the assumed primary atomization scaling on the predicted spray structure to be assessed for the first time.

Recent advances in droplet sizing measurement techniques have allowed for quantification of microscopic spray details closer to the atomizing region of the spray. In particular, the ultra-small angle x-ray scattering (USAXS) measurement technique has the capability of quantifying the Sauter mean diameter (SMD) of droplet size distributions, particularly in dense regions of the spray within the near-nozzle region [31-32]. Available USAXS measurements along the spray centerline for dense ambient conditions ($\hat{\rho}$ less than 100) were used to assess spray predictions by the KH spray model [33]. After careful calibration of the breakup time and size constants, the KH spray model was found to match the measured SMD distribution in the central region of the spray over the range of evaluated ambient and injection conditions. However, questions remain if the SMD

distribution in the central and peripheral regions of the spray will continue to scale according to KH theory at lower ambient density conditions ($\hat{\rho}$ greater than 100), or if other physics, such as turbulent primary atomization, will govern the droplet size distribution.

These newly available spray measurements provide a unique opportunity for assessment of primary atomization models through their influence on the predicted droplet size distribution throughout the spray. In order to identify the strengths and deficiencies of existing spray breakup models, we evaluate the response of predicted spray structure from three different spray models, namely the KH, KH-ACT, and newly developed KH-Faeth model, to changes in injection and ambient conditions. More specifically, we identify unique metrics to characterize the response of droplet distributions along the central and peripheral regions of the spray to changes in injection and ambient conditions. Using local sensitivity analysis, we compare the response of the predicted spray structure among the three primary atomization models, and evaluate the relationship of the selected response metrics to the employed primary atomization model. We compare our findings with experimental measurements, where available, and draw conclusions regarding the necessary improvements to the existing primary atomization models. Finally, we conclude with a list of experimental conditions and measurements that can provide critical information to guide the development of improved spray atomization and secondary droplet breakup models that can be applied throughout the engine cycle.

Experimental Spray Model Validation Data

Experimental and simulated conditions used in this work to study the spray structure of non-vaporizing diesel sprays are detailed in Table 1. Two single-hole injectors from the Engine Combustion Network (ECN), namely the Spray A and Spray D injector nozzles are utilized in this work [34-35]. All experiments were based on the use of nominally-matched single-orifice axial spray injectors, available to participants of the ECN. Rate-of-injection (ROI) [36-38], liquid penetration [34], and USAXS [32] measurements are employed for boundary condition definition and primary atomization model assessment. Discussion of the experimental data sets can be found below.

Table 1. Ambient and injection conditions for non-vaporizing Engine Combustion Network [34] Spray A and Spray D nozzles modeled in this work.

Experimental Parameter	Spray A #210675		Spray D #209133	
Nozzle diameter (d_{noz}) [μm]	89.4		187	
Nozzle Discharge Coefficient (C_d)	0.89		0.90	
Injection Duration [ms]	6.00		4.69	
Total Injected mass [mg]	15.2		51.6	
Nozzle K-factor	1.5		3.7	
Fuel	n-dodecane			
Fuel Temperature [K]	363			
ANL Ambient Temperature [K]	303			
SNL Ambient Temperature [K]	440			
Ambient Composition	100% N_2			
Ambient Density (ρ_g) [kg/m^3]	22.8	7.6	2.4	1.2
Density Ratio ($\hat{\rho} = \rho_f/\rho_g$)	32.7	98.0	310.4	620.8
Fuel Injection Pressure [MPa]	50		150	

Rate of Injection and Nozzle Flow Characterization

ROI profiles for Spray A and Spray D nozzles, as shown at the reference condition of $\hat{\rho}$ = 32, P_{inj} = 150 MPa in Figure 1, are used to define the injection velocity boundary condition in the spray simulations. Details regarding the nozzle flow coefficients and total injected mass are detailed in Table 1. The Spray A ROI was obtained from Centro Motores Térmicos (CMT) virtual injector model [37-38], using nozzle geometry specifications for the ECN Spray A nozzle #210675 [35]. The Spray D ROI profile was obtained from rate-of-momentum measurements conducted in Georgia Tech's spray combustion chamber using the impingement technique for ECN nozzle #209133, along with measurements of total collected mass over 50 injections. Details regarding the experimental measurement technique, uncertainty quantification, and spray vessel can be found in previous works from Georgia Tech [39-41].

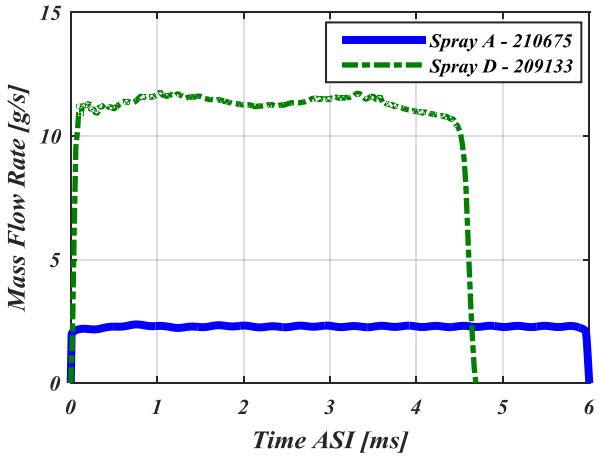

Figure 1. Comparison of the Engine Combustion Network Spray A [37-38] and Spray D measured rate of injection at $\hat{\rho}$ = 32 and P_{inj} = 150 MPa.

Liquid Penetration Data

Measurement of the liquid penetration, as shown in Figure 2, was conducted for the ECN Spray A nozzle #210677, under the reference condition of $\hat{\rho}$ = 32 and P_{inj} = 150 MPa. The liquid penetration data was obtained using the Schlieren technique at Sandia National Labs in their constant volume spray vessel [34]. Further details regarding the experimental set-up and spray vessel are detailed in the previous works from Sandia National Labs [42]. While the majority of experimental measurements presented and utilized in this work were conducted under atmospheric ambient temperature conditions (303 K), liquid penetration measurements at Sandia were performed at a slightly higher ambient temperature (440 K) environment. The ambient temperature is still lower than the boiling temperature for n-dodecane (489 K at 1 bar), and therefore the effects of vaporization on the spray penetration are expected to be minimal. Therefore, the measured liquid penetration can be used for comparison against model predictions at the reference condition, as will be shown and discussed later, to ensure that the momentum exchange between the liquid phase fuel and ambient gases is well captured by each of the spray models.

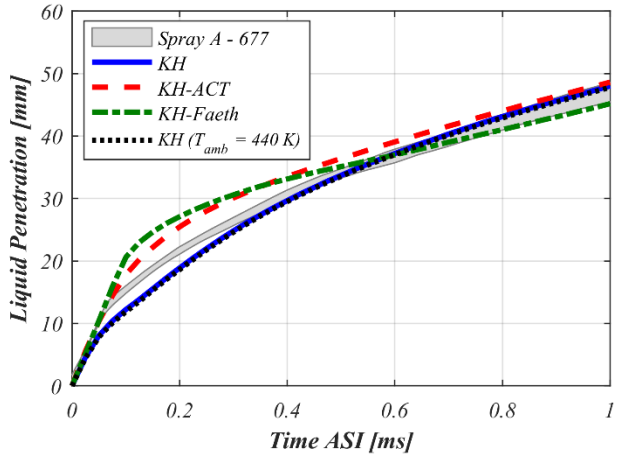

Figure 2. Comparison of measured liquid penetration [34] against predicted liquid penetration for all three spray models based on 99% accumulated mass metric at $\hat{\rho}$ = 32, P_{inj} = 150 MPa for the ECN Spray A nozzle.

Spray Centerline Droplet Sizing Measurements

USAXS measurements quantifying SMD distribution along the spray centerline, as shown in Figure 3, were obtained at the Advanced Photon Source using ECN Spray A nozzle #210675 [32]. A 100x500 µm x-ray beam is passed through the spray, with a resultant x-ray scattering detected as a function of scattering angle in order to determine the differential scattering cross section. When these measurements of differential scattering cross section are evaluated with co-located x-ray radiography measurements, SMD of the droplets in the sampled region can be determined. The measurements begin 1 mm from the injector nozzle and extend downstream along the spray centerline. Further details regarding the experimental measurement technique and spray chamber can be found in previous publications from Argonne National Labs [31-32].

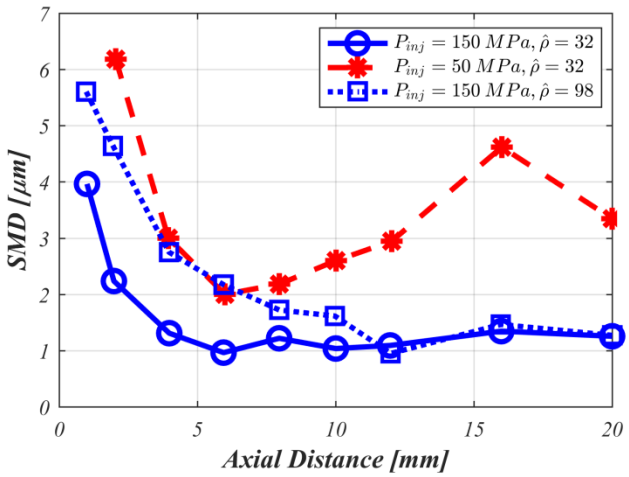

Figure 3. Comparison of axial distributions of USAXS SMD measurements [32] along the spray centerline for ECN Spray A nozzle #210675. Experimental measurements were conducted for $\hat{\rho}$ less than 100, and P_{inj} between 50 and 150 MPa.

In general, the SMD measurements indicate the presence of large droplets in the near nozzle region that rapidly decrease in size due to spray and droplet breakup processes. For each of the measurement conditions, a minimum SMD (SMD_{min}) can be found to characterize the droplet size distribution along the spray axis. Decreases in P_{inj} are also observed to produce relatively larger droplets, and increases in SMD with axial distance, which is likely due to the combined effect of increased probability of droplet coalescence, aerodynamic drag forces, and the momentum of larger droplets surpassing slower moving neighboring droplets [43]. Across all of the measured conditions, it is evident that decreases in P_{inj} result in relatively larger droplet sizes along the spray axis, while decreases in ρ_g (and therefore increases in $\hat{\rho}$) have minimal effect on the SMD_{min} along the spray centerline.

Computational Modeling

Three different primary atomization models are evaluated, namely KH, KH-ACT and the newly developed KH-Faeth model, in order to evaluate the influence of atomization on predicted spray structure throughout the spray. The CFD spray model set-up is described below.

CFD Code

The commercial CFD code, CONVERGE [44], was utilized to simulate the injection of an n-dodecane spray into a constant volume chamber at non-vaporizing conditions, as listed in Table 1. The spray combustion chamber was modeled using a three-dimensional hexahedral structured mesh, as shown in Figure 4. A large domain was selected in order to model a free fuel jet, where the wall effects are insignificant within the timescales and regions of interest. Fixed embedding was employed with additional levels of refinement in the near-nozzle region to resolve the flow near the injector. Using two levels of Adaptive Mesh Refinement (AMR), the grid can be further refined outside of this region for the velocity field. Based on the grid convergence study presented in previous work by the authors [45], a grid with a minimum cell size of 125 µm was selected for this study.

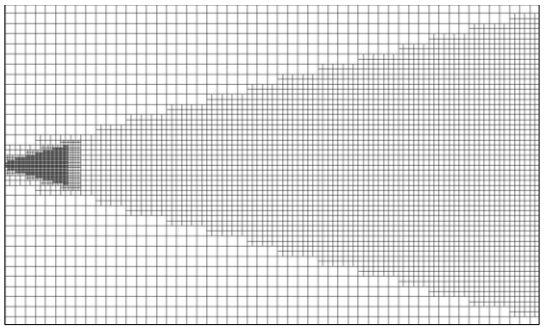

Figure 4. Central slice of computational mesh of the constant volume spray chamber at the center of the spray at the beginning of the simulation. Using different levels of fixed embedding and adaptive mesh refinement, the three-dimensional mesh is composed of a maximum of 1.7 million cells, with a minimum cell size of 125 µm.

The ROI profiles for the Spray A injector [37-38] and for the Spray D injector, shown in Figure 1, and nozzle discharge coefficients, C_d, listed in Table 1, were used to calculate the injection velocities at the nozzle exit. In order to yield better mass distribution in the near-nozzle region, liquid mass is injected within a circle instead of at a point source [46], where the radius of the circle is equal to the nozzle radius. Using the "blob" injection model [14], 1 million computational parcels were injected to represent the dense spray. The Reynolds-Averaged Navier-Stokes (RANS) approach, using a

standard k-ε turbulence model [47] with a turbulent round-jet correction [48], is utilized to describe the ambient gas-phase flow field. Three different models to represent the spray primary atomization process are evaluated in this work, namely the Kelvin-Helmholtz (KH) aerodynamic-induced breakup model [17], the KH-Aerodynamics-Cavitation-Turbulence (KH-ACT) hybrid primary atomization model [24], and the newly developed KH-Faeth hybrid primary atomization model. The model formulations will be briefly described below. For all primary atomization models, secondary droplet breakup is modeled using the KH model. As a result, these three spray models are therefore identical in set-up, except for the employed primary atomization sub-model.

Primary Atomization Model Formulations

As will be shown later, the KH, KH-ACT and KH-Faeth models predict unique droplet size distributions in the near-nozzle region because of the different characteristic length and time scales governing the physical mechanisms of primary atomization. For the KH primary atomization model, the breakup of the injected fuel is modeled via KH aerodynamic instabilities, with primary droplet formation governed by the following physical model equations [17]:

$$\frac{da}{dt} = \frac{-a - r_c}{\tau_{KH}} \tag{1}$$

$$\tau_{KH} = \frac{3.726 B_1 a}{\Lambda_{KH} \Omega} \tag{2}$$

$$r_c = B_0 \Lambda_{KH} \tag{3}$$

where, a and r_c are the radius of the "parent" blob and "child" droplets, respectively, τ_{KH} is the KH characteristic primary breakup timescale, Ω is the maximum growth rate of the most unstable liquid surface wave, with corresponding wavelength, Λ_{KH}, and B_0 is a break-up constant with a conventional value of 0.61. Recent work by the authors has demonstrated that calibrating B_0 to a value of 1.0 can improve droplet size predictions in the central region of the spray [33]. The primary empirical constant employed in the KH break-up model is the time constant, B_1, which is widely calibrated to a number between 1.76 and 100 [49]. Increases in B_1 serve to increase the time required for injected droplets to decrease in size to the child droplet size, r_c, as defined in Equation (3).

The KH-ACT model is a hybrid primary atomization model [24], which evaluates the competing mechanisms of KH aerodynamic instabilities, as previously described, and turbulence-induced breakup. The characteristic length (L_t) and time (τ_t) for turbulence-induced breakup are assumed to scale with the turbulent integral length scale, as originally proposed by Huh and Gosman [18]:

$$L_t(t) = C_\mu \frac{K(t)^{1.5}}{\varepsilon(t)} \tag{4}$$

$$\tau_t(t) = C_\mu \frac{K(t)}{\varepsilon(t)} \tag{5}$$

where K and ε are the instantaneous turbulent kinetic energy and dissipation rate, and C_μ is one of the model constants employed in the k-ε turbulence model [47]. Initial turbulence levels at the nozzle exit, k_0 and ε_0, are determined by a force balance between the pressure force exerted on the liquid at the nozzle exit and turbulent stress within the nozzle [18, 22]. Turbulence levels then evolve according to the liquid phase standard k-ε turbulence model as the computational parcel convects downstream. At each time step, for every computational parent parcel, the KH and turbulent primary breakup rates are calculated and compared, and the maximum breakup rate is selected as the dominant primary atomization mechanism.

$$\frac{L_A}{\tau_A} = max\{\frac{a - r_c}{\tau_{KH}}, \frac{L_t(t)}{\tau_t(t)}\} \tag{6}$$

If KH primary breakup is dominant, then the parent parcels evolve according to Equation (1). However, if turbulent primary breakup dominates the atomization process, then the parent parcel decreases in size according to the following relation:

$$\frac{da}{dt} = -C_{T,CAV} \frac{L_A}{\tau_A} \tag{7}$$

where $C_{T,CAV}$ is the breakup rate calibration constant. It should be noted that though the KH-ACT model includes a cavitation-induced breakup timescale, which competes with the aerodynamic and turbulence breakup rates to determine the dominant primary atomization mechanism, cavitation-induced primary breakup was not modeled in this computational study. The Spray A injector has been shown to suppress cavitation phenomenon for $\hat{\rho}$ less than 100 [50], and the nozzle flow characterization of the Spray D injector also suggests suppression of cavitation under similar conditions [36]. However, more work is needed to characterize nozzle flows at these higher $\hat{\rho}$ conditions, where the ambient pressure is expected to fall below the fuel vapor pressure, which could enhance the possibility of cavitation [26, 51]. For now, this computational study proceeds with a focus on the influence of nozzle-generated turbulence and the growth of hydrodynamic instabilities on the primary atomization process and resultant predicted spray structure.

In order to understand how sensitive the predicted spray structure is to the representation of the turbulence-induced breakup process, we have developed a new hybrid primary atomization model approach, called the KH-Faeth model; in this model, the turbulent length and time scales are modeled using empirical correlations from the work of Faeth and co-workers [29]. The salient conclusions of their work that support their correlations are highlighted here.

Based on an extensive database of near-nozzle holography imaging measurements across a wide range in liquid Reynolds number, Re_f, (9 x 10^4 – 5.3 x 10^5) and $\hat{\rho}$ (104-6230) conditions, Faeth and co-workers developed a phenomenological framework to describe the onset of turbulent breakup and subsequent droplet formation process for round turbulent liquid jets injected into quiescent gases. For liquid jets injected into atmospheric conditions, they found that breakup scaled purely with the nozzle exit turbulence properties. However, for $\hat{\rho}$ less than 500, they found that aerodynamic effects can enhance spray breakup. They hypothesize that this enhanced breakup occurs due to a local reduction in pressure due to acceleration of the ambient gas over surface protuberances that originate from liquid turbulence, akin to flow over a sphere [29]. Note that this mechanism of aerodynamically-enhanced breakup is distinct from the aerodynamically-induced breakup mechanism of surface wave development and growth that is represented in the KH breakup model. Using an energy balance between the mechanical energy at the liquid surface due to aerodynamic effects, the kinetic energy from the turbulent velocity fluctuations, and the surface energy at the

instant of droplet formation, it was found that the measured size of ligaments and droplets formed, L_{Faeth}, were of the same order as estimated eddy scales within the inertial sub-range of the turbulence spectrum. It should be noted that this correlation will therefore result in the formation of droplets that are smaller than those predicted by the KH-ACT model, where the turbulent length scale is assumed to be proportional to the integral length scale.

Based on their analysis of the measured liquid surface ligament and droplet properties at the onset of turbulent breakup, the time required to form a droplet, τ_{Faeth}, was found to be proportional to the time required for a droplet to form from a ligament of size L_{Faeth}, according to the Rayleigh instability mechanism. For low Ohnesorge liquids, where viscosity effects can be neglected, Wu and Faeth [29] determined that $\tau_{Faeth} \alpha \sqrt{\rho_f (L_{Faeth})^3/\sigma}$. In the KH-Faeth model, we implement a similar definition for τ_{Faeth}:

$$\tau_{Faeth} = C_\tau \sqrt{\frac{\rho_f (L_{Faeth})^3}{\sigma}} \tag{8}$$

where C_τ is the turbulent breakup time constant, and σ is the surface tension of the liquid in the ambient gas. In the present study, C_τ is assumed to equal unity.

Wu and Faeth also developed a correlation to relate L_{Faeth} to nozzle exit turbulence properties and the axial location, *x*, where droplets are formed from the turbulent breakup process [29]. By assuming that the stream-wise velocity of the droplet-forming eddy remains relatively constant and can be equated to the injection velocity, U_{inj}, *x* is simply equal to the product of U_{inj} and τ_{Faeth}. By using Equation (8) and re-arranging the terms, L_{Faeth}, can be determined with the following relation:

$$\frac{L_{Faeth}}{\Lambda} = C_{sx} \left(\frac{x}{\Lambda We_{f\Lambda}^{1/2}} \right)^{\frac{2}{3}} \tag{9}$$

where Λ is the radial integral length scale, C_{sx} is an empirical constant, and $We_{f\Lambda}$ is the Λ-based liquid Weber number ($\rho_f U_{inj}^2 \Lambda/\sigma$). Based on experimental data across a wide range of Re_f (9 x 10^4 – 5.3 x 10^5) and $\hat{\rho}$ (104-6230) conditions, Wu and Faeth determined that the empirical correlation in Equation (9) best fit the entire experimental data set when C_{sx} was set to 0.65.

In the KH-Faeth model, τ_{Faeth} and L_{Faeth} are used to represent the characteristic time and length scale governing the turbulence-induced primary breakup process. The turbulence-induced breakup model is implemented in a construct similar to the KH-ACT model. At each time step, only one primary atomization mechanism, either KH or turbulence-induced breakup, is assumed to act upon the computational parent parcel. KH and turbulent primary breakup rates are calculated and compared, and the maximum breakup rate is selected as the dominant primary atomization mechanism.

$$\frac{L_A}{\tau_A} = max\{\frac{a - r_c}{\tau_{KH}}, \frac{L_{Faeth}}{\tau_{Faeth}}\} \tag{10}$$

Similar to the KH-ACT atomization model, if KH primary breakup is dominant, then the parent parcels evolve according to Equation (1). However, if turbulent primary breakup dominates the atomization process, then the parent parcel decreases in size according to Equation (7).

For each of the three spray model set-ups, after a child droplet has been formed from the selected primary atomization process, the droplet may undergo subsequent secondary droplet breakup due to the KH instability if the droplet size is larger than Λ_{KH}.

Spray Model Calibration and Set-Up

Spray model constants, listed in Table 2, were tuned to match the predicted SMD distribution by the KH and KH-ACT models with the USAXS measurements along the spray centerline. Time-averaged two-dimensional SMD distributions were calculated by evaluating the droplet size distribution across the width of the spray within 0.25mm wide bins from 0.7 to 1.0 ms ASI. Comparison between predicted and measured SMD at the reference condition for the Spray A nozzle, where $\hat{\rho}$ = 32 and P_{inj} = 150 MPa, is shown in Figure 5(a). For the hybrid KH-Faeth atomization model, the model constants for the KH aerodynamic breakup model equations were set equal to those used in the KH and KH-ACT models. However, no additional tuning was performed for the calibration constants within the Faeth turbulent primary breakup correlations (Equations (8) and (9)). We elected to refrain from ad-hoc tuning of these equations in this initial study of the model formulation for two reasons: 1) the Faeth empirical formulations are based on fits to experimental data that cover a reasonably wide range of conditions [29], and 2) the current work seeks to focus on predicted atomization response trends, rather than magnitude, as an initial assessment of the usefulness of this new modeling approach. As a result, as seen in Figure 5(a), the KH-Faeth model underpredicts SMD. Because the Spray A reference condition occurs at a denser ambient condition than the conditions evaluated in the work of Faeth and co-workers ($\hat{\rho}$ greater than 100) [29], it could be expected that extrapolation of their empirical correlations would not yield good agreement with measurements at these conditions. In future work, additional droplet sizing validation data will become available within the central and peripheral regions of the spray under high ambient density conditions, and we will evaluate the appropriateness of implementing additional or modified calibration constants to the hybrid KH-Faeth model.

Table 2. Key spray model constants describing the three different spray model set-ups.

Model Parameters	Model Set-Up
B_1	60.0
B_0	1.0
C_μ	0.09
$C_{T,CAV}$	0.33
C_τ	1.0
C_{sx}	0.65

This computational study seeks to compare the predicted spray structure and its sensitivity to changes in injection and ambient conditions among the three primary atomization models considered. It is worth noting that this comparison is conducted for a fixed set of spray model constants across the entire range of evaluated ambient and injection conditions. It is likely that the response of the model to changes in injection and ambient conditions may be dependent on the spray model constants employed. The authors acknowledge this potential dependency as an important factor to consider when interpreting the results of this work. However, calibration of the KH,

KH-ACT and KH-Faeth spray models have been informed and justified with the best available experimental data. As additional experimental data become available, calibration of the spray models, and their implications on the predicted spray structure, can be re-evaluated.

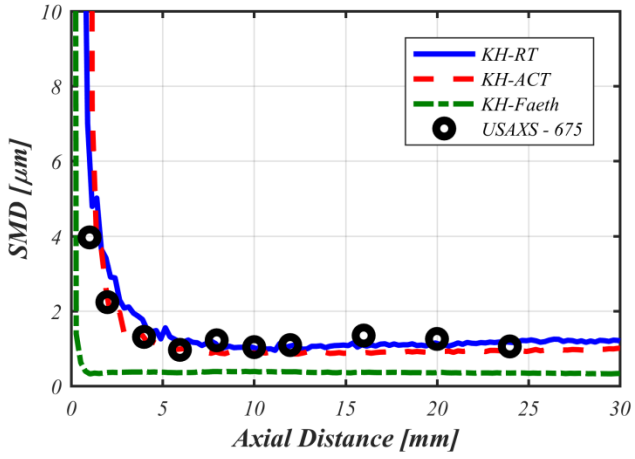

(a)

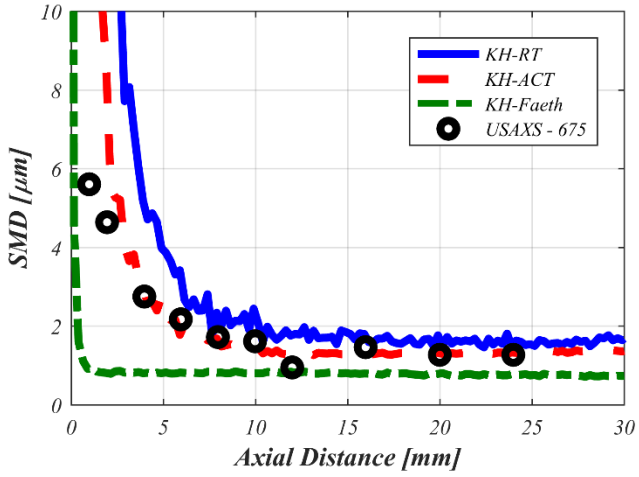

(b)

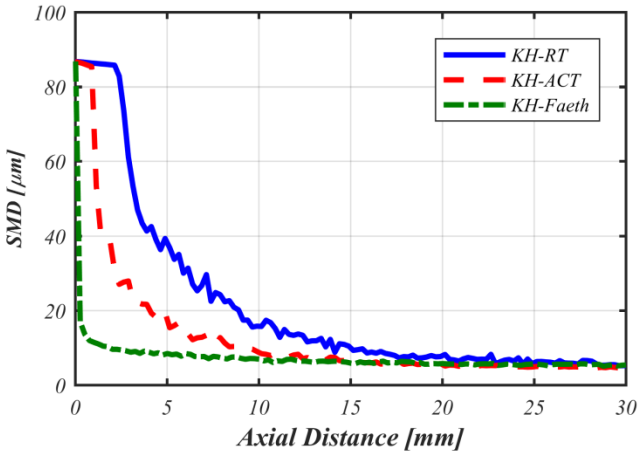

(c)

Figure 5. Axial distributions of SMD along the spray centerline are compared among the three spray models for the Spray A nozzle at P_{inj} = 150 MPa and (a) $\hat{\rho}$ = 32, (b) $\hat{\rho}$ = 98, and at (c) $\hat{\rho}$ = 620.

It is important to ensure that the model set-ups well represent not only local spray details, such as SMD along the spray centerline, but also global spray features, such as liquid penetration. Comparison between the measured and predicted liquid penetration for the Spray A nozzle is shown in Figure 2. Ideally, as proposed in [52] for the vaporizing Spray "A" condition, a physically-based metric, such as the local liquid volume fraction, should be employed to define the computational liquid boundary for comparison against liquid penetration measurements. However, in absence of well-defined modeling practices for non-vaporizing sprays, the predicted liquid penetration was defined as the downstream axial location where 99% of the total injected mass has been encompassed. The model predictions of liquid penetration are within the experimental uncertainty of the measured liquid penetration within the steady portion of injection, from 0.7 to 1.0 ms after start-of-injection (ASI). Additionally, as shown in Figure 2, the predicted spray penetration was evaluated at a higher ambient temperature of 440 K to match the conditions from the experimental measurements conducted at Sandia [34]. The nearly identical predictions between the two spray simulations confirms the minimal influence of vaporization on the predicted spray penetration at the 440K ambient temperature condition. Agreement among model predictions and the experimental data indicates that the momentum exchange between the liquid phase fuel and ambient gases is well predicted within this time frame. It should be noted that during the early injection transient period, differences are seen among the predicted liquid penetration among the three models; this difference highlights the dependence of start of injection spray development on the details of the initial breakup process. However, since our computational study focuses on the study of predicted spray structure within the steady portion of injection (0.7 to 1.0 ms ASI), it is determined that each of the spray model set-ups are capable of representing the global and local features of the spray.

Results and Discussion

In this work, we compare the dependence of the predicted spray structure on the employed primary atomization model. We first identify response metrics that can efficiently characterize the predicted droplet size distribution throughout the spray to simplify

the model analysis and comparisons of complex three-dimensional droplet field predictions. Then, using local sensitivity analysis, we compare the prediction of these response metrics among the three primary atomization models considered in this work to changes in injection and ambient conditions. Comparison of model predictions with available experimental measurements help identify key experimental measurements and conditions that are needed to inform the improvement of spray primary atomization and secondary droplet breakup models.

Identification of Response Metrics

In order to understand how the assumed primary atomization mechanism affects the predicted spray structure, it is desirable to identify simplified metrics that can enable insight into the behavior of the selected primary atomization model over a wide range of operating conditions. Additionally, the selected response metrics must also be directly comparable to available experimental measurements of droplet size. Example time-averaged SMD distributions, as predicted by the KH model for the ECN Spray A nozzle, are displayed in Figure 6. In Figure 6(a), the SMD distribution is shown for the $\hat{\rho}$ = 32, P_{inj} = 150 MPa condition. The droplets begin with diameter approximately equal to the nozzle diameter (89.4 μm) and quickly decrease in size due to primary atomization and secondary droplet breakup.

Along the centerline, the droplets eventually reach a stable droplet size near 6 mm from the nozzle exit. This behavior is also seen for the predicted SMD distribution even at the lower ambient density condition ($\hat{\rho}$ = 620, P_{inj} = 150 MPa), as shown in Figure 6(b), although the stable droplet size is not reached until approximately 40 mm from the nozzle exit. Similar to the experimental trends seen in the USAXS measurements in Figure 3 for $\hat{\rho}$ less than 100, the minimum droplet size formed along the spray centerline, SMD_{min} is approximately equal to the stable droplet size. Therefore, to characterize the droplet size evolution in the central region of the spray, the minimum SMD (SMD_{min}) along the spray centerline is selected as the target parameter for the basis of comparison among all three models, and with available USAXS measurements, as defined in Equation (11) below,

$$SMD_{min} = min\{SMD(x, y = 0)\} \quad (11)$$

where x is the axial distance from the nozzle, and y is the transverse distance, where y = 0 represents the spray centerline.

Along the periphery of the spray, the predicted droplet size distribution exhibits a sensitivity to changes in $\hat{\rho}$ that differs from the predicted SMD along the spray centerline. At the $\hat{\rho}$ = 32 condition as shown in Figure 6(a), the droplet sizes along the periphery of the spray are very similar to those along the centerline. As a result, the SMD distribution appears relatively "flat" throughout the spray. However, at higher $\hat{\rho}$ conditions, this "flat" SMD distribution is not exhibited, as can be seen by the larger droplets along the periphery of the spray, relative to the centerline, in Figure 6(b).

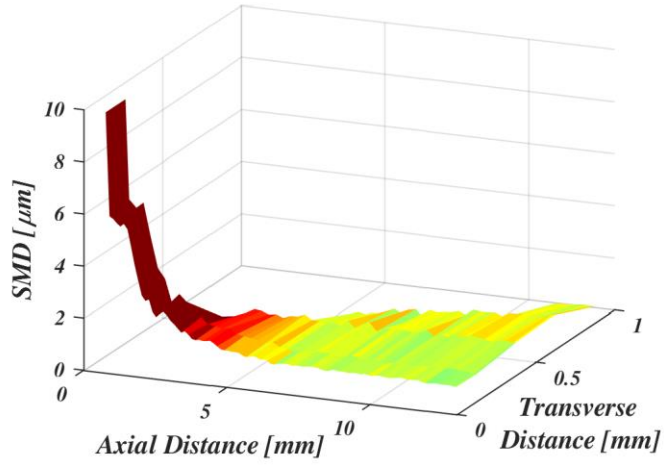

(a)

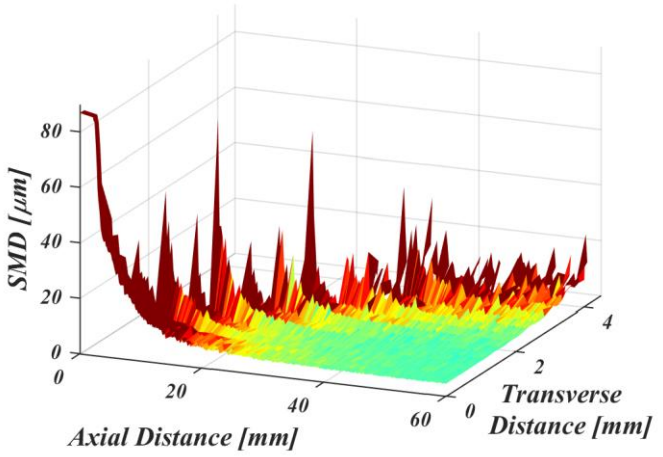

(b)

Figure 6. Sample 2-D time-averaged SMD map as predicted by the KH model for the Spray A nozzle at ambient and injection conditions of (a) $\hat{\rho}$ = 32, P_{inj} = 150 MPa and (b) $\hat{\rho}$ = 620, P_{inj} = 150 MPa. Only half of the spray is shown in order to clearly illustrate the difference in predicted SMD between the central and peripheral regions of the spray.

There are several reasons why this change in droplet size behavior is seen at the higher $\hat{\rho}$ condition. As $\hat{\rho}$ is increased from 32 to 620, the primary atomization timescale increases, as illustrated by the relatively slower rate of SMD decrease along the spray centerline in Figure 6(b). At the $\hat{\rho}$ = 32 condition in Figure 6(a), the SMD along the centerline decreases by more than 95% of its initial size within the first 2 mm from the nozzle exit, whereas the SMD along the centerline decreases by less than 5% within the same distance at the $\hat{\rho}$ = 620 condition (Figure 6(b)). At 2 mm from the nozzle exit at the $\hat{\rho}$ = 32 condition, the primary atomization process has completed. Within this same distance, the velocity of the liquid jet has not developed substantially and is approximately uniform across the width of the spray. Therefore, all computational parcels across the width of the spray encounter similar local conditions and undergo similar subsequent changes in droplet size due to secondary droplet breakup. As a result, the droplet size distribution across the width of the spray at downstream locations is relatively constant. In contrast, at the $\hat{\rho}$ = 620 condition, the primary atomization process is substantially elongated. Therefore, computational parcels across the width of the spray encounter different local conditions as they

continue to decrease in size due to the development of the velocity profile of the spray. For example, parcels along the centerline of the spray have larger relative velocities and continue to undergo secondary droplet breakup. However, along the periphery of the spray, the relative velocities of the parcels approach zero, which results in nearly infinite droplet breakup times, and serve to "freeze" the droplet sizes. Therefore, relatively larger droplet sizes can be seen along the periphery of the spray in comparison to those along the spray centerline.

These results suggest that in absence of droplet interactions, droplet size distributions across the width of the spray may provide indirect indication of the primary atomization process, as noted in previous work by the authors [33]. Similar droplet sizes in the central and peripheral regions of the spray were formed from a fast primary atomization process. In contrast, a non-uniform droplet size distribution, with larger droplets along the periphery, was formed from an elongated primary atomization process that was more strongly affected by the fully-developed spray velocity profile. As will be discussed later, there are currently no available measurements that can assess this predicted relationship between the atomization timescale and the resultant downstream droplet size distribution. However, complementary measurements of the characteristic timescale or axial length of the primary atomization region and two-dimensional droplet size distributions could yield valuable insight into the currently missing link between the atomization processes in the near nozzle region and the produced spray structure.

Because the predicted droplet size distributions are seen to strongly differ in behavior along the centerline and periphery of the spray, it is desirable to quantify the peripheral droplet size distribution with its own response metric that will enable rapid insight into the behaviors of different primary atomization models over a wide range of operating conditions. It is also desirable to target a quantity that may be feasibly measured to enable model validation of these behaviors. For example, conventional PDPA measurement techniques can provide point measurements in these regions [53]. Our group is also actively developing a 2-D droplet size measurement technique for diesel sprays, applicable to the optically thin spray periphery [33]. A representative response metric to characterize the periphery of the spray can be identified through evaluation of the peripheral droplet size distribution, as shown in Figure 6(b). The peripheral SMD distribution varies greatly in the first 40 mm from the injector nozzle exit. Downstream of 40mm, the peripheral SMD distribution does not appreciably change with axial distance. This steadiness in the peripheral SMD distribution is seen to coincide with the axial locations, $\tilde{x}$, where the central SMD distribution also reaches a steady value within 10% of SMD_{min}. As a result, characterization of the peripheral droplet distribution is limited to axial locations, $\tilde{x}$. Additionally, across the range of conditions and evaluated spray models, it was determined that the key features of the peripheral droplet size distribution were contained in transverse regions of the spray, $\tilde{y}$, where the local SMD distribution deviates by more than 20% from the centerline SMD. As a result, for the best comparison of spray model predictions with available and emerging measurements along the periphery of the spray, the arithmetic mean of the peripheral SMD distribution, SMD_{periph}, is identified as the characteristic response metric. $\tilde{x}$, $\tilde{y}$, and SMD_{periph} can be mathematically defined with the following equations:

$$\tilde{x} = \{x | 0.9SMD_{min} \leq SMD(x, y = 0) \leq 1.1SMD_{min}\} \quad (12\text{-a})$$

$$\tilde{y} = \{y | SMD(\tilde{x}, y) \geq 1.2SMD(\tilde{x}, y = 0)\} \quad (12\text{-b})$$

$$SMD_{periph} = mean\{SMD(\tilde{x}, \tilde{y})\} \quad (12\text{-c})$$

Local Sensitivity Analysis of SMD_{min} to Changes in Ambient and Injection Conditions

Using the selected response metrics to characterize the spray structure in the central (SMD_{min}) and peripheral (SMD_{periph}) regions of the spray, it is possible to efficiently evaluate how the predicted spray structure responds to changes in injection and ambient conditions for each spray model. Comparison of SMD_{min} across the entire condition space is shown in Figure 7 for the (a) KH, (b) KH-ACT, and (c) KH-Faeth primary atomization models. For each spray model, SMD_{min} at each condition is normalized by the SMD_{min} predicted by the KH model at the reference condition at $\hat{\rho}$ = 620 and P_{inj} = 150 MPa for Spray D with d_{noz} = 187 μm, to yield $\overline{SMD}_{min}$. This normalization enables the response of the models to be evaluated relative to each other. Decreases in $\overline{SMD}_{min}$ indicate the formation of relatively smaller droplets along the centerline of the spray, and an enhanced spray breakup process. Comparison of Figure 7(a), (b) and (c) reveals that all models exhibit the same general trend that $\overline{SMD}_{min}$ (and therefore SMD_{min}) decreases with decreasing $\hat{\rho}$, increasing P_{inj}, and decreasing d_{noz}.

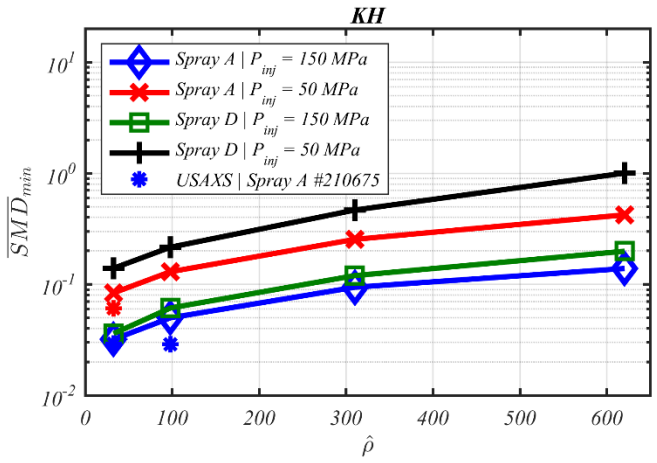

(a)

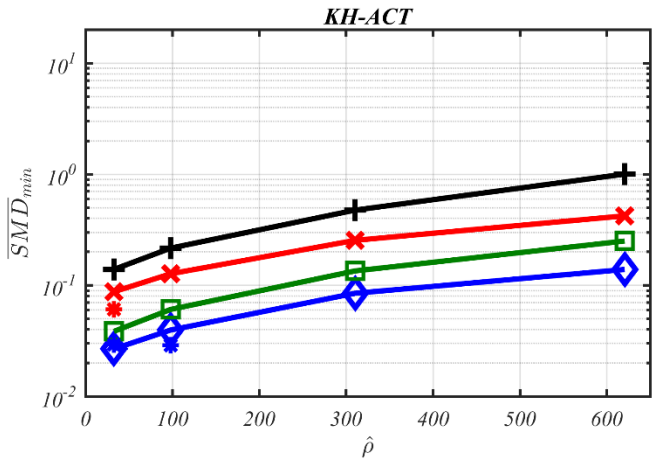

(b)

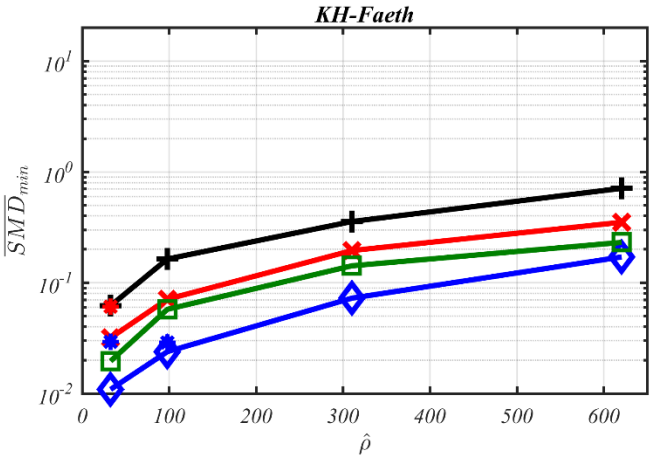

(c)

Figure 7. Comparison of $\overline{SMD}_{min}$ as predicted by (a) KH, (b) KH-ACT, and (c) KH-Faeth models over range of $\hat{\rho}$, P_{inj}, and d_{noz}. $\overline{SMD}_{min}$ based on USAXS measurements are colored according to the nozzle and injection pressure condition. Decreases in $\overline{SMD}_{min}$ indicate the formation of relatively smaller droplets along the centerline of the spray, and an enhanced droplet breakup process.

A non-intuitive result is found when comparing the KH and KH-ACT spray models; in particular, the two models predict similar responses of SMD_{min} to changes in ambient and injection conditions, even though the KH-ACT model includes additional physics that represent the effect of nozzle-generated turbulence on the primary atomization process. In fact, for the set of spray model constants employed in this study, as listed in Table 2, and over the range of evaluated conditions, the turbulent primary breakup governs the size of droplets predicted by the KH-ACT model in the near nozzle region. Indeed, as shown in Figure 5, the KH-ACT model is seen to produce smaller SMD in the near nozzle region relative to the KH model predictions. These findings are also in agreement with the work from Tatschl and co-workers [54], who found that the turbulent breakup rate is much higher in the near nozzle region than that due to the growth of hydrodynamic instabilities. However, the turbulent primary atomization process does not yield smaller SMD_{min} than that produced by the aerodynamic primary atomization model. Instead, the droplet sizes formed from the turbulent breakup process scale with the turbulent integral length scale, which results in droplets that are larger than Λ_{KH}. These droplets are therefore unstable, undergo subsequent KH secondary breakup, and ultimately result in SMD_{min} which scale with Λ_{KH}, as opposed to L_t. Therefore, the details of primary atomization in the near nozzle region appear to have minimal effect on SMD_{min} in the downstream portion of the spray. This scaling yields good agreement among the KH and KH-ACT model predictions and available USAXS measurements along the spray centerline, as shown in Figure 7(a) and (b) for $\hat{\rho}$ less than 100. This agreement suggests that the experimentally measured SMD_{min} scales with Λ_{KH} for $\hat{\rho}$ less than 100, and is ultimately controlled by secondary droplet breakup and may not be sensitive to the details of the primary atomization process.

In general, while the KH-Faeth model SMD_{min} predictions, shown in Figure 7(c), exhibit similar trends with respect to changes in injection and ambient conditions, the KH-Faeth model predicts smaller SMD_{min} than either the KH or KH-ACT models for $\hat{\rho}$ less than 100. Indeed as previously shown in Figure 5(a)-(b), the KH-Faeth primary atomization model produces relatively smaller droplets in the first few millimeters from the nozzle exit. These findings are to be expected based on the employed scaling from the Faeth correlation, where droplet sizes formed from the primary atomization process scale within the inertial subrange of the turbulence spectrum [29]. This is contrast to the scaling of larger droplets from the KH-ACT model, which scale with the integral length scale [18, 24]. At the $\hat{\rho}$ = 98 condition, as shown in Figure 5(b), the KH-Faeth model predicts the formation of SMD_{min} that is consistent with the USAXS measurements. However at ambient conditions where $\hat{\rho}$ is greater than 100, as shown in Figure 5(c), the KH-Faeth primary atomization model produces droplets that are larger than Λ_{KH}. As a result, these droplets are unstable to KH instabilities and undergo subsequent droplet breakup. For $\hat{\rho}$ greater than 100, the KH-Faeth predictions for SMD_{min} generally scale with Λ_{KH} and closely match those predicted by the KH and KH-ACT models, as illustrated in Figure 5(c) and Figure 7.

It is important to note that for the lowest ambient densities considered in this study ($\hat{\rho}$ = 620), particularly for the Spray D cases, the stable droplet size and SMD_{min} in the central region of the spray are formed at distances greater than 60 mm from the injector nozzle. One of the important reasons SMD_{min} is a critical response metric is because of its potential relationship to the secondary droplet breakup process. However, the link between droplet breakup and SMD_{min} becomes complicated if the effects of droplet interactions, such as collisions and coalescence, are important. Over the span of 60 mm or more (greater than 300 nozzle diameters for the Spray D injector nozzle), it is possible that droplet interactions could influence the size of droplets measured along the spray centerline. However, as the spray disperses and entrains more ambient gas, the liquid volume fraction, and therefore droplet number density, will decrease with distance from the injector. As the droplet number density decreases, the average distance between droplets will increase, resulting in a decreased probability of droplet interaction [55]. As a result, it is likely that SMD_{min} may still be correlated with the secondary droplet breakup process.

In summary, for this computational study, we find that SMD_{min} is determined by a competition between the primary atomization and subsequent droplet breakup length scales. As expected, the predicted SMD_{min} by the KH model scales with Λ_{KH} across all injection and ambient conditions. Even with the addition of a turbulence-induced primary atomization mechanism to the KH model, the droplet sizes formed from the KH-ACT primary atomization model are larger than Λ_{KH} and are therefore unstable and undergo subsequent KH droplet breakup; as a result, the predicted SMD_{min} by the KH-ACT model is the result of KH droplet breakup and therefore scales with Λ_{KH} across all injection and ambient conditions. In contrast, the scaling of SMD_{min} predicted by the KH-Faeth model exhibits a dependence on ambient condition. For $\hat{\rho}$ less than 100, the turbulence-induced primary atomization process, as modeled with the Faeth correlation (Equation (9)) [29], produces droplets that are smaller than Λ_{KH}. As a result, these droplets are stable and SMD_{min} scales with the Faeth turbulent length scale correlation, as described in Equation (9). For $\hat{\rho}$ greater than 100, the turbulent primary atomization process produces droplets that are larger than Λ_{KH}. As a result, these droplets are unstable to KH instabilities and SMD_{min} ultimately scales with Λ_{KH}.

Local Sensitivity Analysis of SMD_{periph} to Changes in Ambient and Injection Conditions

Similar analysis of the predicted spray structure in the central region of the spray is extended to characterize the predicted droplet size distribution along the periphery of the spray. Comparison of

SMD_{periph} across the entire range of injection and ambient conditions is shown in Figure 8 as predicted by the (a) KH, (b) KH-ACT and (c) KH-Faeth primary atomization models. Similar to $\overline{SMD}_{min}$, SMD_{periph} at each condition is normalized by SMD_{periph} predicted by the KH model at the reference condition at $\hat{\rho}$ = 620 and P_{inj} = 50 MPa for Spray D with d_{noz} = 187 µm, to yield $\overline{SMD}_{periph}$. This normalization allows for the relative influence of injection and ambient conditions to be evaluated on the peripheral droplet size distribution among the three primary atomization models. For all of the models, with a fixed nozzle diameter and P_{inj}, the predicted $\overline{SMD}_{periph}$ (and therefore SMD_{periph}) increases with increasing $\hat{\rho}$. Additionally, all models predict an increase in SMD_{periph} when d_{noz} is increased, for a fixed P_{inj} and $\hat{\rho}$.

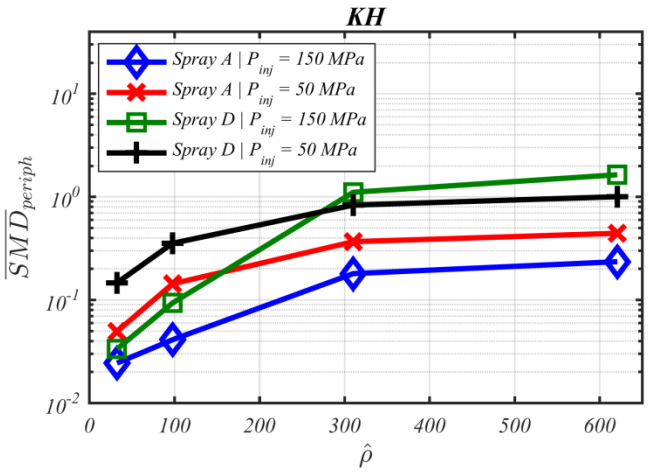

(a)

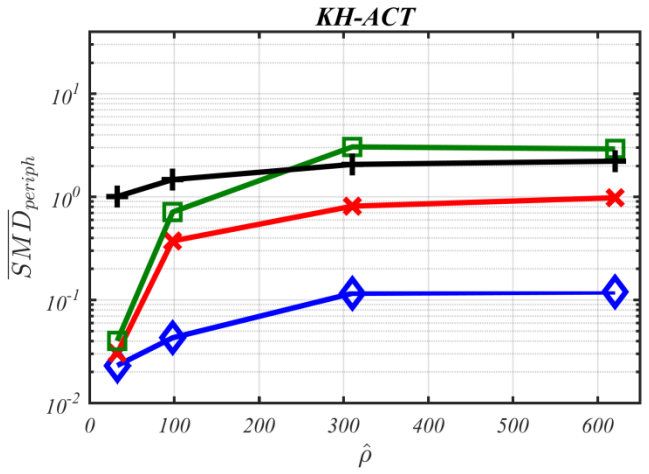

(b)

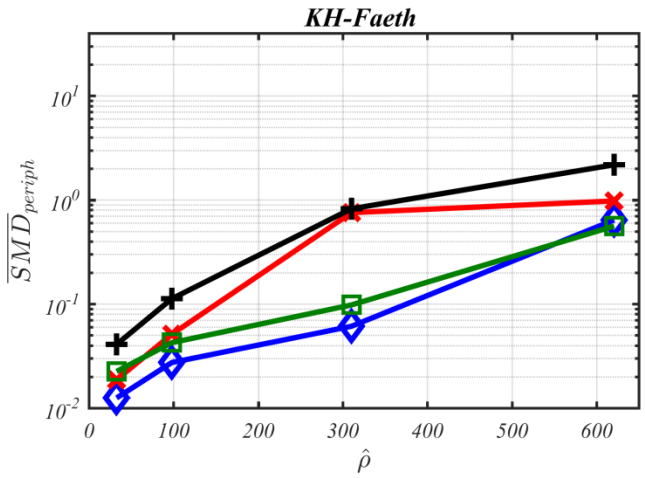

(c)

Figure 8. Comparison of $\overline{SMD}_{periph}$ as predicted by (a) KH, (b) KH-ACT, and (c) KH-Faeth models over range of $\hat{\rho}$, P_{inj}, and d_{noz}.

The SMD_{periph} predicted by the KH-Faeth model exhibits a much smaller sensitivity to changes in d_{noz} than is predicted by either the KH or KH-ACT model. As previously noted, in the absence of droplet-droplet interactions, droplet size distributions across the width of the spray provide indirect validation of the primary atomization process. The droplets formed from the KH-Faeth primary atomization model scale with turbulent eddies within the inertial subrange. This scaling differs from that employed in the KH-ACT model, where droplets formed form the primary atomization process scale with turbulent eddies within the energy-containing range of the turbulence spectrum, which have a larger dependence on geometric features of the flow, such as d_{noz} [56].

The difference in sensitivity of SMD_{periph} to changes in d_{noz} predicted by the three spray models is amplified at ambient conditions where $\hat{\rho}$ is greater than 100. At these conditions, the length and time scales characterizing aerodynamic breakup become insensitive to changes in $\hat{\rho}$. This insensitivity is exhibited by the relatively constant predictions of SMD_{periph} by the KH and KH-ACT models in Figure 8(a) and (b) for $\hat{\rho}$ greater than 100 and for all d_{noz} and P_{inj} considered. As a result, these higher $\hat{\rho}$ ambient conditions present a prime set of experimental conditions where droplet sizing measurements along the periphery of the spray should be focused. Quantifying the measured response of SMD_{periph} to changes in d_{noz} and $\hat{\rho}$ at these conditions may help identify modeling inaccuracies of existing spray models. These measurements also show promise of shedding light on an appropriate primary atomization mechanism that can unify the spray breakup modeling approach across the entire range of ambient conditions. However, the link between primary atomization and SMD_{periph} becomes complicated if the effects of droplet interactions, such as collisions and coalescence, are important.

Differences also exist between the response of the predicted SMD_{periph} to changes in P_{inj} for a fixed d_{noz} and $\hat{\rho}$. For example, for the Spray A nozzle conditions shown in Figure 8, all of the models predict an increase in SMD_{periph} when P_{inj} is decreased from 150 MPa (blue line) to 50 MPa (red line) across all $\hat{\rho}$ conditions. This relationship between SMD and P_{inj} is consistent with the predicted trends for SMD_{min} for all models, as shown in Figure 7. For the Spray D nozzle, the KH-Faeth model predicts a similar trend for SMD_{periph} across all $\hat{\rho}$ conditions: when P_{inj} is decreased from 150 MPa (green line) to 50 MPa (black line), SMD_{periph} increases. This trend is also

exhibited for the KH and KH-ACT spray predictions at $\hat{\rho}$ conditions less than 100 for the Spray D nozzle. However for $\hat{\rho}$ greater than 100, the trend is reversed: decreases in P_{inj} result in smaller predicted SMD_{periph} by the KH and KH-ACT models.

Although this trend contradicts the response of SMD_{min} to changes in P_{inj}, the relationship can be better understood by evaluating sample two-dimensional SMD distributions for the Spray D nozzle as predicted by the KH-ACT model. The KH-ACT predicted spray structure is shown in Figure 9, at a condition of $\hat{\rho}$ = 310 and (a) P_{inj} = 50 MPa and (b) P_{inj} = 150 MPa. As P_{inj} is increased, the primary atomization timescale remains approximately constant, as illustrated by the similar rates of SMD decrease along the spray centerline in Figure 9(a) and (b). Additionally, the atomization process is noted to be relatively longer than that observed at lower $\hat{\rho}$ conditions (Figure 6(a)). More specifically, the computational parcels have only decreased in size by less than 5% within the first 3 mm from the nozzle. As a result, computational parcels across the width of the spray are expected to undergo different local flow conditions as they continue to decrease in size due to the development of the spray velocity profile, which produces a non-uniform droplet size distribution downstream. This predicted non-uniform spray structure is consistent with the sample droplet size distribution predicted by the KH model for the Spray A nozzle, as previously shown in Figure 6(b) at $\hat{\rho}$ = 620, P_{inj} = 150 MPa. It is worth noting that evaluating these SMD distributions over a larger time-averaging window (from 0.7 to 1.5 ms ASI) yields minimal differences in the predicted SMD distribution.

For the lower injection pressure case in Figure 9(a), a stable droplet size is achieved along the central region of the spray between 40 to 60 mm from the nozzle exit. The corresponding peripheral region shows a wide range of SMD, ranging from 25 µm to 150 µm. As P_{inj} is increased, the transit time of the computational parcel decreases and high momentum computational parcels from the edge of the primary atomization region convect downstream at a faster rate than at the lower P_{inj} condition. As a result, a higher probability of SMD greater than 100 µm can be seen at the higher P_{inj} condition along the periphery of the spray in Figure 9(b). This effect is amplified by the low relative velocities of droplets along the periphery of the spray, which does not promote KH secondary breakup. As a result, the timescale for secondary droplet breakup approaches infinity and causes a nearly "frozen" SMD distribution along the periphery. This trend is also observed in the SMD predictions by the KH model. The presence of larger SMD_{periph} with increases in P_{inj} is not observed in the model predictions at lower $\hat{\rho}$ conditions due to the combined effect of faster primary atomization, and increased inertia of the ambient gas acting on the droplets, which serves to decrease the momentum of droplets along the periphery. Additionally, this trend is not observed for Spray A conditions due to the combined effects of a faster primary atomization process and production of smaller droplets, which have relatively lower momentum than those formed from the Spray D injector nozzle.

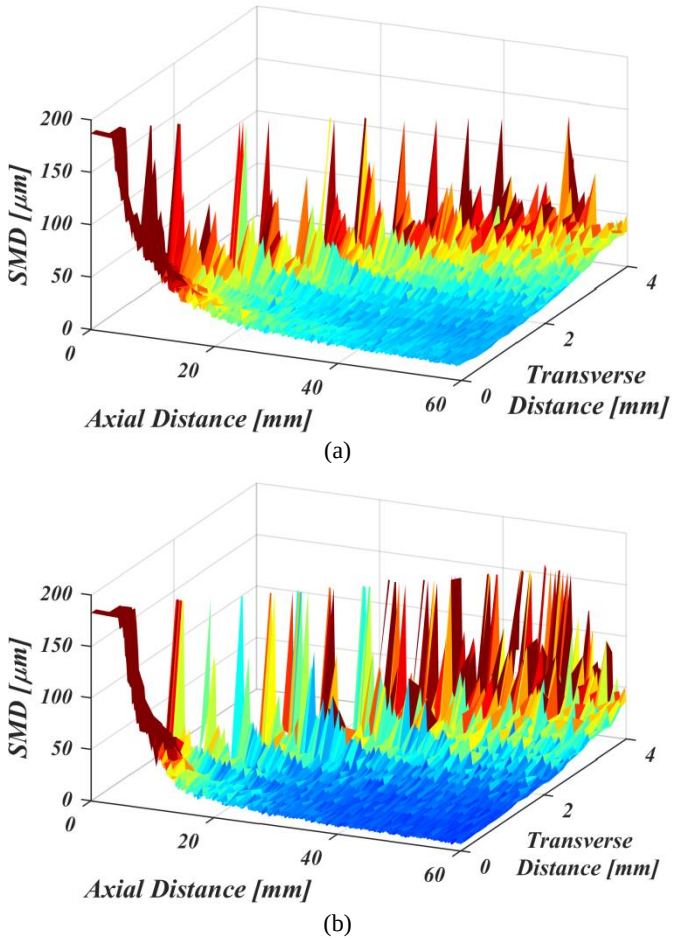

Figure 9. Sample 2-D time-averaged SMD map as predicted by the KH-ACT model for the Spray D nozzle at ambient and injection conditions of (a) $\hat{\rho}$ = 310, P_{inj} = 50 MPa and (b) $\hat{\rho}$ = 310, P_{inj} = 150 MPa. Only half of the spray is shown in order to clearly illustrate the difference in predicted SMD between the central and peripheral regions of the spray.

Experimental Measurements Needed for the Improvement of Spray Model Predictions

Recent developments in droplet sizing techniques show promise of providing valuable information regarding the response of droplet sizes along the central and peripheral regions of the spray to changes in injection and ambient conditions. Available USAXS measurements for the ECN Spray A #210675 nozzle at $\hat{\rho}$ conditions less than 100 show good agreement with SMD_{min} predicted by the KH model, as shown in Figure 7(a). This agreement suggests that SMD_{min} scales with Λ_{KH} for $\hat{\rho}$ less than 100. However, additional measurements for the larger Spray D nozzle in this range of $\hat{\rho}$ would strengthen arguments regarding the extension of this observed scaling to other nozzle sizes. Droplet size measurements along the spray centerline are also currently missing for $\hat{\rho}$ greater than 100. Application of the USAXS measurement technique [31-32] to this range of ambient conditions would yield insight into the appropriate scaling of SMD_{min}, and whether the scaling of SMD_{min} with Λ_{KH} should extend to lower ambient densities.

Currently, there are no other available SMD measurements for the ECN nozzles modeled in this work that can help validate the distinct two-dimensional behaviors observed. However, there are several

available experimental techniques that could provide valuable insight into the sensitivity of droplet size distributions in the peripheral regions of the spray to changes in injection and ambient conditions. For example, long distance microscopic imaging can quantify spatial and temporal distributions of droplet size along the periphery of the spray under certain limited conditions [4-5]. Crua and co-workers have optimized the experimental set-up and have been able to achieve droplet size resolutions down to 2 μm. However, this technique may not be able to quantify droplet sizes for the Spray A nozzle at the lowest $\hat{\rho}$ conditions considered in this work, where model predictions indicate the presence of droplets less than 2 μm along the periphery. However, this measurement technique shows promise of providing valuable information for higher $\hat{\rho}$ conditions for the Spray D nozzle, where droplet sizes along the periphery are predicted to be greater than 4 μm. Additional experimental techniques that can also quantify spatial distributions of the peripheral droplet size distribution are USAXS [31-32], dual-wavelength extinction [33, 57], and PDPA [53]. Experimental measurements conducted at $\hat{\rho}$ conditions greater than 100 would help address observed modeling discrepancies in the predicted response of SMD_{periph} to changes in $\hat{\rho}$, P_{inj}, and d_{noz}, as shown in Figure 8(a)-(c). Exploration of the measured sensitivity of SMD_{periph} to changes in injection and ambient conditions would provide critical information in understanding the physics governing the peripheral droplet size distribution.

Complementary to the peripheral droplet sizing measurements, measurements of the characteristic timescale or axial length of the primary atomization region would yield critical information regarding processes in the near nozzle region and its influence on the peripheral droplet size distribution. To date, there are no existing measurements that can quantify the primary atomization timescale for diesel like sprays. However, there are some experimental techniques which show promise of characterizing the length of the primary atomization region through quantification of the dense liquid mass distribution expected in this region. In particular, the application of computed tomography to x-ray radiography measurements allows for the characterization of liquid volume fraction distributions, particularly in the dense regions of the spray. In recent work by Duke and co-workers, almost 100 different viewing angles were used to reconstruct the liquid volume fraction distribution of a multi-hole gasoline spray from the measured fuel mass density distributions [58]. Such a large number of viewing angles are required to characterize spray asymmetries and reduce the uncertainty in the computed tomographic reconstruction. For the ECN Spray A and Spray D single-hole injectors considered in our computational study, it is likely that fewer viewing angles would be required to achieve adequate measurements of the liquid volume fraction distribution in the near nozzle region. However, to date, the maximum number of viewing angles for x-ray radiography has been limited for high-pressure fuel sprays; for the Spray A injector, the maximum number of reported viewing angles has been four [3]. As improvements are made to the x-ray radiography experimental set-up to optimize data acquisition for high-pressure fuel sprays, this type of measurement may become more feasible in providing such information about the internal structure of the near-nozzle region. Ultimately, experimental characterization of near-nozzle spray formation processes under engine-relevant conditions is necessary to improve our understanding for how the spray breakup process should be modeled.

Summary/Conclusions

In order to advance the predictive capability of spray models for use in engine CFD codes, there is a serious need to address modeling inaccuracies in representing the atomization and spray formation process. An informed pathway towards predictive spray models is only possible through detailed characterization of the predicted spray structure from existing spray models, in concert with comparison and validation against quantitative droplet sizing measurements throughout the spray. In this computational study, we explored the influence of the primary atomization model on the predicted spray structure through evaluation of two existing spray models in the literature, namely the KH and KH-ACT models, and a newly developed KH-Faeth model. A wide range of injection and ambient conditions for two different ECN nozzles (Spray A and Spray D) were studied in this work. Different or opposing responses of the predicted droplet size distribution to changes in injection and ambient conditions motivated the selection of critical experimental measurements and conditions to address model uncertainties. Comparison between predicted spray structure among the three primary atomization models and against available spray measurements revealed:

1. For all three primary atomization models, the predicted droplet sizes in the central and peripheral regions of the spray exhibited different sensitivities and responses to changes in injection and ambient conditions considered in this study. As a result, unique response metrics were identified for the central and peripheral droplet size distributions to comprehensively characterize the influence of the spray primary atomization model on the predicted spray structure. The minimum SMD (SMD_{min}) along the spray centerline was used to characterize droplet sizes in the central region of the spray, and provided a direct comparison with available USAXS measurements. The mean SMD along the spray periphery (SMD_{periph}) was used to characterize droplet sizes in the peripheral region of the spray, and will enable a direct comparison with two-dimensional maps of the SMD distribution when peripheral droplet sizing measurements become available.

2. Comparison of predicted SMD_{min} among the three models revealed that the droplet sizes along the central region of the spray are determined through a competition between the size of droplets formed from the primary atomization and secondary droplet breakup processes. For $\hat{\rho}$ greater than 100, secondary droplet breakup, as modeled with the KH instability mechanism, was observed to control the size of droplets in the central region of the spray. For $\hat{\rho}$ less than 100, the KH and KH-ACT models both predict SMD_{min} that scale with the KH length scale. However, the KH-Faeth model predicts the formation of droplets that are smaller than the droplet breakup length scale for $\hat{\rho}$ less than 100. As a result, droplets in the central region of the spray remain stable in size and instead scale with the Faeth primary atomization length scale. However, comparison with available USAXS measurements for $\hat{\rho}$ conditions less than 100 revealed that the Faeth turbulent primary atomization scaling predicted a more intense breakup process than indicated in the measurements. Potential calibration of the KH-Faeth model will be explored in the future when additional droplet size measurements are available in the central and peripheral regions of the spray.

3. Comparison of predicted SMD_{periph} among the three models revealed that the droplet sizes along the spray periphery are highly dependent upon the details of the primary atomization process, particularly the atomization timescale. A fast primary atomization process results in SMD_{periph} that largely scale with SMD_{min}. For elongated primary

atomization processes, SMD_{periph} generally scale with the characteristic atomization length scale. This observed relationship presents motivation for utilizing droplet sizing measurements along the periphery of the spray as an indirect characterization of the unobservable primary atomization process.

4. Through comparison of the predicted spray structure among the three spray models and against available measurements, experimental measurements were identified that would help determine spray modeling inaccuracies and appropriate scalings for the droplet formation and breakup processes. The only measurement technique currently capable of performing droplet sizing measurements in the optically-thick center of the spray is the USAXS technique. Presently, USAXS measurements are only available for the ECN Spray A nozzle under $\hat{\rho}$ less than 100. Application of the measurement technique to larger nozzles, like the ECN Spray D nozzles, and to higher $\hat{\rho}$ conditions would allow for improved insight into how droplet sizes in the central region of the spray should behave to changes in ambient and injection conditions. To characterize the two-dimensional behavior of the SMD distribution observed in this work, we identified several experimental techniques that are capable of characterizing the peripheral droplet size distribution, including USAXS and long distance microscopy.

This computational study has demonstrated different scalings and sensitivities of droplet sizes in the central and peripheral regions of the spray to changes in injection and ambient conditions. Although this work explored the competing effects of the employed aerodynamic and turbulent primary atomization models on the predicted spray structure, future work should evaluate how and under what conditions cavitation might influence central and peripheral droplet size distributions. Results from future joint computational and experimental studies show promise of yielding insight into the appropriate physics that should be included to model diesel-like sprays over a wide range of operating conditions.

References

1. Lefebvre A. H., "Atomization and Sprays," (New York, Taylor and Francis, 1989).
2. Reitz, R.D., and Bracco, F.V., "Mechanism of atomization of a liquid jet," *Physics of Fluids*, 25(2):1730-1741, 1982.
3. Pickett, L., Manin, J., Kastengren, A., and Powell, C., "Comparison of Near-Field Structure and Growth of a Diesel Spray Using Light-Based Optical Microscopy and X-Ray Radiography," *SAE Int. J. Engines* 7(2):1044-1053, 2014.
4. Crua, C., Heikal, M., and Gold, M., "Dropsizing of Near-Nozzle Diesel and RME Sprays by Microscopic Imaging," *12th Triennial International Conference on Liquid Atomization and Spray Systems*, Heidelberg, Germany, 2012.
5. Crua, C., Heikal, M., and Gold, M., "Microscopic imaging of the initial stage of diesel spray formation," *Fuel*, 157:140-150, 2015.
6. Linne, M., Paciaroni, M., Hall T., and Parker, T., "Ballistic imaging of the near field in a diesel spray," *Experiments in Fluids*, 40(6): 836-846, 2006.
7. Gorokhovski, M., and Herrmann, M., "Modeling Primary Atomization," *Annual Review of Fluid Mechanics*, 40: 343-366, 2008.
8. Desjardins, O., and Pitsch, H., "Detailed Numerical Investigation of Turbulent Atomization of Liquid Jets," *Atomization and Sprays*, 20(4): 311-336, 2010.
9. Bode, M., Diewald, F., Broll, D., Heyse, J. et al., "Influence of the Injector Geometry on Primary Breakup in Diesel Injector Systems," *SAE Technical Paper* 2014-01-1427, 2014.
10. Subramaniam, S., "Lagrangian-Eulerian Methods for Multiphase Flows," *Prog. Energy Combust. Sci.*, 39(2-3): 215-245, 2013.
11. Amsden, A.A., O'Rourke, P.J., and Butler, T.D., "KIVA–II: A Computer Program for Chemically Reactive Flows with Sprays," *Technical Report* LA–11560–MS, Los Alamos National Laboratory, 1989.
12. O'Rourke, P.J., "The KIVA computer–program for multidimensional chemically reactive fluid–flows with fuel sprays," *Lecture Notes in Physics*, 241: 74– 89, 1985.
13. Reitz, R.D., and Diwakar, R., "Structure of High-Pressure Fuel Sprays," *SAE Technical Paper* 870598, 1987.
14. Dukowicz, J. K., "A Particle-Fluid Numerical Model for Liquid Sprays," *Journal of Computational Physics*, 1980.
15. Reitz, R.D. "Atomization and other breakup regimes of a liquid jet," PhD Thesis, Princeton University, 1978.
16. Ranz, W.E., "Some experiments on orifice sprays," *The Canadian Journal of Chemical Engineering*, 36(4): 175-181, 1958.
17. Reitz, R.D., "Modeling Atomization Processes in High-Pressure Vaporizing Sprays," *Atomisation and Spray Technology*, 3: 309-337, 1987.
18. Huh, K.Y., and Gosman, A.D., "A phenomenological model of diesel spray atomization," *Proceedings of the International Conference of Multi-Phase Flows*, Tsukuba, Japan, 1991.
19. Reitz, R.D., and Bracco, F.V., "On the dependence of spray angles and other spray parameters on nozzle design and operating conditions," *SAE Technical Paper* 790494, 1979.
20. Hiroyasu, H., and Kadota, T., "Fuel droplet size distribution in diesel combustion chamber," *SAE Technical Paper* 740715, 1974.
21. Yule, A.J., Mo, S.L., Tham, S.Y., and Aval, S.M., "Diesel Spray Structure," *Proceedings of the Third International Conference on Liquid Atomization and Spray Systems*, London, England, 1985.
22. Huh, K.Y., Lee, E., and Koo, J., "Diesel Spray Atomization Model Considering Nozzle Exit Turbulence Conditions," *Atomization and Sprays*, 8(4): 453-469, 1998.
23. Som, S., and Aggarwal, S.K., "Assessment of Atomization Models for Diesel Engine Simulations," *Atomization and Sprays*, 19(9):885-903, 2009.
24. Som, S., Ramirez, A.I., Aggarwal, S.K., Kastengren, A.L. et al., "Development and validation of a primary breakup model for diesel engine applications," *SAE Technical Paper* 2009-01-0838, 2009.
25. Som, S., and Aggarwal, S.K., "Effects of primary breakup modeling on spray and combustion characteristics of compression ignition engines," *Combustion and Flame*, 157:1179-1193, 2010.
26. Som, S., "Development and Validation of Spray Models for Investigating Diesel Engine Combustion and Emissions," PhD Thesis, University of Illinois at Chicago, 2009.
27. Wang, J., "X-ray vision of fuel sprays," *J. Synchrotron Radiation*, 12:197–207, 2005.
28. Yue, Y., Powell, C.F., Poola, R., Wang, J., and Schaller, J.K., "Quantitative measurements of diesel fuel spray characteristics in the near-nozzle region using x-ray absorption," *Atomization and Sprays*, 11:471–490, 2001.

29. Wu, P.-K., and Faeth, G.M., "Aerodynamic Effects on Primary Breakup of Turbulent Liquids," *Atomization and Sprays*, 3:265-289, 1993.
30. Faeth, G.M., and Wu, P.-K., "Structure and breakup properties of sprays," *International Journal of Multiphase Flow*, 21:99-127, 1995.
31. Powell, C.F., Duke, D. et al., "Measurements of Diesel Spray Droplet Size with Ultra-Small Angle X-Ray Scattering," *25th Annual Conference on Liquid Atomization and Spray Systems*, Pittsburgh, PA, 2013.
32. Kastengren, A., Ilavsky, J., Viera, J.P., Payri, R. et al., "Measurements of Droplet Size in Shear-Driven Atomization Using Ultra-Small Angle X-Ray Scattering," *International Journal of Multiphase Flows*, Under Initial Review.
33. Magnotti, G.M., and Genzale, C.L., "Detailed Assessment of Diesel Spray Atomization Models Using Visible and X-Ray Extinction Measurements," *International Journal of Multiphase Flows*, Under Initial Review.
34. Engine Combustion Network, "Engine Combustion Network Experimental Data Archive," https://ecn.sandia.gov, accessed Oct. 2016.
35. Kastengren, A.L., Tilocco, F.Z., Powell, C.F., Manin, J. et al., "Engine Combustion Network (ECN): Measurements of Nozzle Geometry and Hydraulic Behavior," *Atomization and Sprays*, 22(12): 1011-1052, 2012.
36. Payri, R., Gimeno, J., Cuisano, J., and Arco, J., "Hydraulic characterization of diesel engine single-hole injectors," *Fuel*, 180: 357-366, 2016.
37. Payri, R., Salvador, F.J., Gimeno, J., and Bracho, G., "A new methodology for correcting the signal cumulative phenomenon on injection rate measurements," *Experimental Techniques*, 32(1): 46-49, 2008.
38. Centro Motores Térmicos, "Virtual Injection Rate Generator," http://www.cmt.upv.es/ECN03.aspx#model, accessed Oct. 2016.
39. Knox, B.W., Franze, M.J., Genzale, C.L., "Diesel Spray Rate-of-Momentum Measurement Uncertainties and Diagnostic Considerations," *ASME J. Eng. Gas Turbines Power*, 138(3): 2016.
40. Falcone, J.A., Knox, B.W., and Genzale, C.L., "Identifying Uncertainties in Diesel Spray Rate-of-Momentum Transients Under Elevated Back Pressure," *ASME 2015 Internal Combustion Engine Division Fall Technical Conference*, Houston, Texas, 2015.
41. Knox, B.W., and Genzale, C.L., "Effects of End-of-Injection Transients on Combustion Recession in Diesel Sprays," *SAE Int. J. Engines*, 9(2): 932-949, 2016.
42. Pickett, L., Genzale, C., Bruneaux, G., Malbec, L. et al., "Comparison of Diesel Spray Combustion in Different High-Temperature, High-Pressure Facilities," *SAE Int. J. Engines*, 3(2):156-181, 2010.
43. Liu, A.B., Mather, D., Reitz, R.D., "Modeling the Effects of Drop Drag and Breakup on Fuel Sprays," *SAE Technical Paper 930072*, 1993.
44. Richards, K.J., Senecal, P.K., Pomraning, E., CONVERGE™ (Version 2.1) Manual, Convergent Science Inc., 2013.
45. Magnotti, G.M., and Genzale, C.L., "A Novel Approach to Assess Diesel Spray Models using Joint Visible and X-Ray Liquid Extinction Measurements," *SAE Int. J. Fuels Lubr.* 8(1):167-178, 2015.
46. Senecal, P.K., Pomraning, E., Richards, K.J., Som, S., "Grid-Convergent Spray Models for Internal Combustion Engine Computational Fluid Dynamics Simulations," *Journal of Energy Resources Technology*, 136(1): 2013.
47. Han, Z., and Reitz, R.D., "Turbulence modeling of internal combustion engines using RNG k-e models," *Comb. Sci. Tech.*, 106:267-295, 1995.
48. Pope, S., "An explanation of the turbulent round-jet/plane-jet anomaly," *AIAA Journal*, 16:279-281, 1978.
49. Ning, W., "Development of a next-generation spray and atomization model using an Eulerian-Lagrangian methodology," PhD Thesis, University of Wisconsin-Madison, 2007.
50. Duke, D., Swantek, A., Tilocco, Z., Kastengren, A. et al., "X-ray Imaging of Cavitation in Diesel Injectors," *SAE Int. J. Engines*, 7(2):1003-1016, 2014.
51. Schmidt, D.P., and Corradini, M.L., "The internal flow of diesel fuel injector nozzles: A review," *Int. J. Engine Research*, 2(1): 1-22, 2001.
52. Magnotti, G.M., and Genzale, C.L., "Influence of Liquid Penetration Metrics on Diesel Spray Model Validation," *SAE Technical Paper* 2013-01-1102, 2013.
53. Soare, V., "Phase Doppler Measurements in Diesel Dense Sprays: Optimisation of Measurements and Study of the Orifice Geometry Influence over the Spray at Microscopic Level," PhD Thesis, Universidad Politécnica de Valencia, 2007.
54. Tatschl, R., v. Künsberg-Sarre, C., and v. Eberhard, B., "IC-Engine Spray Modeling – Status and Outlook," *International Multidimensional Engine Modeling User's Group Meeting at the SAE Congress*, Detroit, MI, 2002.
55. Munnannur, A., "Droplet Collision Modeling in Multi-Dimensional Engine Spray Computations," PhD, University of Wisconsin-Madison, 2007.
56. Pope, S.B., "Turbulent Flows," (Cambridge University Press, 2000).
57. Labs, J., and Parker, T.E., "Two-dimensional droplet size and volume fraction distribution from the near-injector region of high-pressure diesel sprays," *Atomization and Sprays*, 16(7): 843-855, 2006.
58. Strek, P., Duke, D., Kastengren, A. et al., "X-Ray Radiography and CFD Studies of the Spray G Injector," *SAE Technical Paper* 2016-01-0858, 2016.

Contact Information

Gina M. Magnotti (Corresponding author)
Email: gina.magnotti@gatech.edu

Dr. Caroline L. Genzale
Email: Caroline.Genzale@me.gatech.edu

Acknowledgments

The authors would like to thank Mr. Yoontak Kim and Dr. Benjamin Knox for providing measurements for the rate of momentum, total injected mass, and nozzle flow coefficients for the ECN Spray D injector nozzle #209133.

We gratefully acknowledge the computing resources provided on Blues, a high-performance computing cluster operated by the Laboratory Computing Resource Center at Argonne National Laboratory.

This material is based upon work supported jointly by the Department of Energy, Office of Energy Efficiency and Renewable Energy (EERE), and the Department of Defense (DOD) under Award Number DE-EE0073333.

Definitions/Abbreviations

ASI	After start of injection
ANL	Argonne National Laboratory
ECN	Engine Combustion Network
KH	Kelvin-Helmholtz
KH-ACT	Kelvin-Helmholtz Aerodynamic-Cavitation-Turbulence
SMD	Sauter mean diameter
SMD_{min}	Minimum Sauter mean diameter along the spray centerline
$\overline{SMD}_{min}$	Normalized SMD_{min} with respect to KH predicted SMD_{min} at $\hat{\rho}$ = 620 and P_{inj} = 50 MPa for the Spray D injector nozzle
SMD_{periph}	Mean Sauter mean diameter along the spray periphery
$\overline{SMD}_{periph}$	Normalized SMD_{periph} with respect to KH predicted SMD_{periph} at $\hat{\rho}$ = 620 and P_{inj} = 50 MPa for the Spray D injector nozzle
SNL	Sandia National Laboratories
USAXS	Ultra-small angle X-ray scattering
d_{noz}	Nozzle diameter
P_{inj}	Fuel injection pressure
Λ	Radial integral length scale
Λ_{KH}	Wavelength of fastest growing KH surface wave
ρ_f	Liquid fuel density
ρ_g	Ambient gas density
$\hat{\rho}$	Liquid-to-gas density ratio (ρ_f / ρ_g)
x	Axial distance from the injector nozzle exit
$\tilde{x}$	Axial distances where the peripheral SMD distribution is evaluated
y	Transverse distance from the central spray-axis
$\tilde{y}$	Transverse distances where the peripheral SMD distribution is evaluated